

# Perspective Aperture Dependency of Netted Radar Target Classification

Michele Vespe, Chris J. Baker, Hugh D. Griffiths  
University College London  
Torrington Place, London, WC1E 7JE

## Abstract

*The Automatic Target Recognition (ATR) performance is strongly aspect dependent. In this paper, this concept is extended to the combination of multiple perspectives sensing the target reflectivity function, yielding a description of the angular nodes displacement influence on the probability of correct classification. The results of two- and three-perspective classifiers on 1-D High Range Resolution (HRR) profiles are also discussed for any possible network topology, showing the valuable performance improvement of an approach which could be incorporated in existing and future systems.*

Keywords: ATR, Multi-Perspective Classification, Netted Radar.

## Introduction

The benefits of a reliable and robust target classification have the potential to radically increase the importance and value of radar systems. The interest in radar target classification has intensified as a consequence of the increase of information available from advanced radar systems. This is mainly due to the backscattered signature having high resolution in range and cross-range. Most of the approaches to classification investigate the exploitation of higher and higher spatial resolutions both in one [1] and two [2] dimensions, or concentrate on the role of polarimetric information (e.g. [2], [3]). The examination of the utility of angular diversity for improving classification performance has only recently been approached [4-6]. This is motivated by the fact that, although the description of target scattering is detailed enough to attempt radar target classification, the reliability of this crucial task is influenced by a number of unpredictable factors - and is poor. This is a consequence of the measurement noise, rotational and translational range

migrations, speckle and other factors affecting the sensed attributes. In addition, global or local occlusions also noticeably challenge the attempts to classify targets reliably. Furthermore, ground vehicles are likely to be found concealed or differently configured: the testing set could present different loads or moving parts orientations (i.e. turret rotation, antenna position). As a consequence, the generalisation process is sensitive to the particular scattering centres spatial distribution of the target as presented during the training phase. Since these confusing features appear for a limited range of aspects a higher correct classification rate is expected when multiple perspectives are involved. As it has been shown in [7], for a monostatic netted radar scenario, the classification performance increases with the number of perspectives. Although the improvements are significant, those benefits are dependent on the location of the nodes with respect to the position of the target and its orientation.

The classification performance using multiple perspectives is discussed using full scale measurements of representative

targets. Principal Component Analysis (PCA) is applied to the features extracted from the target Time Domain reflectivity samples to form the input vector for the classifier. A Feed-forward Artificial Neural Networks (FANN) classifier has been trained to execute the single-perspective stage classification. The resulting partial outcomes are then processed to perform multi-perspective classification. The classification performance is presented showing the influence of the intrinsic symmetries of each target on the correct classification rates. These aspects are also explored at different perspective apertures between nodes in the network, and using two and three perspectives. Multi-perspective classification results are finally described for an airborne implementation.

### **Dataset**

The target description is extracted from a dataset provided by Thales, consisting of a sequence of HRR profiles covering  $360^\circ$  of turntable rotation from Inverse Synthetic Aperture Radar (ISAR) measurements. The transmitted waveform is an LFM pulse and the radar returns are compressed giving 30 cm of range resolution. The depression angle of the antenna ( $\sim 8^\circ$ ) is almost constant for the different measurements. Two consecutive profiles are spaced by only  $2''$  of target rotation and non-coherently averaged. Prior to Zero-Doppler Clutter (ZDC) cancellation, it is usually necessary to align the range profiles. However, here, because the input patterns for recognition are collected from turntable measurements, no additional alignment is needed between training and test profiles. Signatures from four ground vehicles classified as *A*, *B*, *C* and *D* form the sub-population problem.

### **FANN Multi-Perspective Classifier**

In previous research [7], three classifiers were tested in a multi-perspective

environment order to examine any bias introduced by a single algorithm. All three classification approaches showed similar trends of correct classification rate (*CRR*) improvement given by the perspective diversity. The FANN algorithm using the Back-Propagation (BP) learning strategy showed the highest accuracy and lowest computational burden. A traditional single-perspective classifier, after training with a set of templates, is tested with profiles collected from all orientations of the target (neglecting the ones used to train the classifier). In a two-perspective (2-P) scenario, the parameter that distinguishes the node locations is their relative perspective aperture  $\Delta\phi_{1,2}=\phi_2-\phi_1$ . Hence, after fixing  $\Delta\phi_{1,2}$ , the 2-P classifier is tested with all possible pairs of HRR profiles displaced by that angle covering all the possible orientations of the target. This is extended to multi-perspective scenarios.

Each class is represented by a set of 36 range profiles, which are taken approximately every  $10^\circ$  of target rotation. The multi-perspective classifier can be seen as the combination of *N* single-perspective classifiers, whereas the eventual decision is made by processing the partial outputs of each single-perspective stage. For feasible implementation of the algorithm in existing systems, the information about the perspective angular displacements is not processed by the classifier.

### **Feature Extraction**

In order to obtain a better generalisation of the results for possible input vectors not used to train the classifier, features from HRR profiles have been extracted. As a consequence, the intrinsic redundancy of the data is reduced and the model simplified. Furthermore, the classification process becomes particularly consistent with those features effectively characterising the object. After adaptively determining a threshold by measuring the

mean intensity of the target backscattering, the radar length of the target for that particular orientation is measured as the distance between the first and last threshold crossings. This is the first component of the feature vector  $f$ , followed by the measure of the average backscattering of the target. Subsequently,  $M$  triples containing the information of the  $M$  peaks extracted in terms of amplitude, location and width are inserted in the feature vector. If the number of peaks above the threshold is less than  $M$ , the triple is set to zero [8]. Different numbers of peaks have been extracted until the classification process revealed a certain degree of robustness. For  $M=4$ , the feature vector has a dimension of 14 elements, and 52 range bin values make up the raw echo profile.

Subsequently, PCA [9] has been applied to the feature vectors  $f$  to enable the data to be represented in a different vector basis that removes similarities (which therefore do not contribute to the classification process) in terms of the directions presenting the smallest variance in the dataset. After subtracting the mean value of the training set feature vectors, the zero-mean dataset is produced and the covariance matrix  $C$  can be calculated as follows:

$$C = E[(f_n - \bar{f})(f_n - \bar{f})^T] \quad (1)$$

where  $E$  is the expected value. After calculating the eigenvectors of the covariance matrix, the  $K$  most significant eigenvectors with the largest eigenvalues are selected to form the new vector basis  $W$ . The test and training feature vectors can then be transformed as follows:

$$f' = W^T (f_n - \bar{f}) \quad (2)$$

The number of principal components  $K$  is chosen as a function of the correct classification rate achieved.

In/Out	Class A	Class B	Class C	Class D
Class A	75.85	11.19	9.57	3.39
Class B	4.75	80.91	13.26	1.08
Class C	2.81	18.98	69.94	8.27
Class D	12.91	0.76	15.26	71.07

**Table 1:** Single-perspective FANN confusion matrix for the four-class problem on features after PCA

In Table 1 the resulting confusion matrix for  $K = 10$  is shown using a single perspective. The  $CRR$  achieved is 74.4%.

### Netted Radar Topologies

Since the radar targets investigated in this paper are man-made objects, they present a number of 3-D symmetries. Furthermore, the measurements are taken for a low depression angle: the radar system, the target and their relative motion vectors can be assumed on the same plane. This geometry allows considering the 2-D problem and symmetries on the projection plane parallel to the ground plane. If the angular aperture of two perspectives is about  $180^\circ$ , the corresponding profiles might be quite highly correlated. This is due to the  $180^\circ$  symmetry typically exhibited by ground vehicles. This network topology causes a reduction in target characterization and eventually decreases the  $CRR$  benefits brought by the second perspective. However, details such as rear-view mirrors, the antenna position and any non-symmetrical or moving parts, will change the two signatures producing  $CRR$  benefits when compared with single-perspective classifiers.

Figure 1 shows the classification performance as a function of angular separation of two perspectives. The equivalent mono-perspective performance is shown at the  $0^\circ$  and  $360^\circ$  positions.

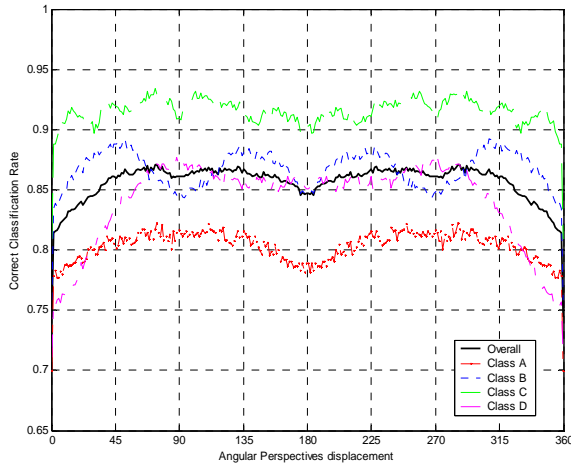


**Figure 1:** Two-perspective correct classification rates versus the angular displacement  $\Delta\phi_{1,2}$

The angular aperture between two signatures in this scenario is the discriminant factor for the combined *CRR*: as the two range profiles decorrelate (i.e.  $\Delta\phi_{1,2}$  increases) the information content of the pair increases. The single target *CRR* shows how the global accuracy depends on the particular geometric features of the target. The drop at  $\Delta\phi_{1,2} = 180^\circ$ , as previously hypothesised, is due to the multiple axes of symmetry of the targets and it is visible for all the classes. Other features appear to be distinctive of the particular target. For example, the class *C* has a number of multiple-bounce phenomena from corner-like scatterers. Their persistency is less than  $15^\circ$ , causing the *CRR* fluctuation. Having  $90^\circ$  of perspective aperture indicates either an improvement or degradation of the target description from a radar backscattering information point of view. This is due to the different intrinsic symmetries and cross similarities exhibited between different classes.

Figure 2 shows the overall *CRR* as a function of the perspective apertures in a three-perspective network. The first perspective is fixed whilst the other two slide around the target completing  $360^\circ$ . These are shown as a function of the angular displacement  $\Delta\phi_{1,2}$  between the

second and the first node, and  $\Delta\phi_{1,3}$  between the third and the first node. The origin of the graph represents the mono-perspective case ( $CRR = 0.74$ ) and it offers a metric for evaluating the *CRR* improvements given by the three perspectives. The directions  $\Delta\phi_{1,2} = \Delta\phi_{1,3}$  correspond to two out of three systems sensing the same perspective, while its parallels symbolise two perspectives displaced by  $90^\circ$  and  $180^\circ$  respectively.

In a 2-P scenario, if the two nodes viewed the target from the same perspective (i.e. the two radars have the same LOS) it would have given the mono-perspective classification rates. In a three-perspective network this would decrease the *CRR* because of the double weighting of a single perspective. As a result, the performance when  $\Delta\phi_{1,2} = 0^\circ$  and  $\Delta\phi_{1,3} \neq 0^\circ$  is worse than the 2-P configuration that simply neglects one of the coinciding perspectives. The node locations corresponding to the higher *CRR* are different from the 2-P case: they appear for the network covering  $120^\circ$  around the target by equally separated nodes, i.e. for the network topologies:  $\Delta\phi = \{\Delta\phi_{1,2}; \Delta\phi_{1,3}\} = \{60^\circ; 120^\circ\}$ ,  $\{60^\circ; 300^\circ\}$  and so forth. Correct classification rates are also maximised when the nodes are equally displaced by  $120^\circ$ , that is  $\Delta\phi = \{120^\circ; 240^\circ\}$ .

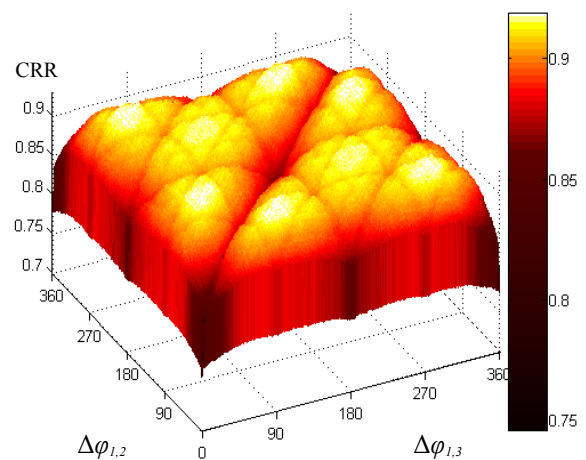


**Figure 2:** Three-perspective correct classification rates versus the angular displacements  $\Delta\phi_{1,2}$  and  $\Delta\phi_{1,3}$

Nevertheless, the difference between the maximum and average classification rates is about 1%.

### Airborne Multi-Perspective Application

A possible application of the multi-perspective classification approach can be identified with the multiple signatures collected by an airborne system flying past the target. If a circular trajectory is covered around the object of interest, the ISAR geometry can be assumed as an approximation of the problem. In a real scenario, the non-circular trajectory would change the distance to the target and therefore the SNR with the consequence of having different quality descriptions of the target depending on the perspective. On the other hand, having an arbitrary trajectory would change the depression angle with the result of decorrelating the perspectives more than at constant elevation, yielding better multi-perspective performance.

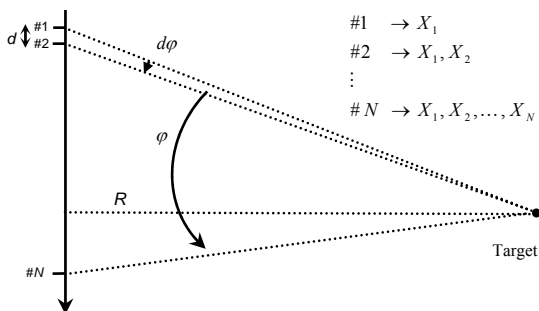


Figure 3: Flying-past geometry for a linear trajectory

Assuming an aircraft flying a linear trajectory as in Figure 3, at a velocity of 200 m/s at a range  $R = 10$  km from the target and transmitting  $n = 8$  chirps using stepped-frequency compression techniques at  $PRF = 3$  kHz, the number of collected signatures at the same centre frequency and polarisation, after averaging over 4 profiles would be  $N \sim 45$  per second, that is one profile every  $d = 4.4$  m. A multi-perspective classifier can be implemented on a cumulative basis, i.e. the HRR profiles  $X_1, X_2, \dots, X_N$  are continuously collected and

progressively presented to the classifier or on an interrupted basis, i.e. the profiles are taken from ad hoc perspectives, chosen according to the best CRR suggested by the multi-perspective graphs (Figure 1 and 2). Between consecutive collections the system can be switched off, reducing the probability of being detected by passive sensors.

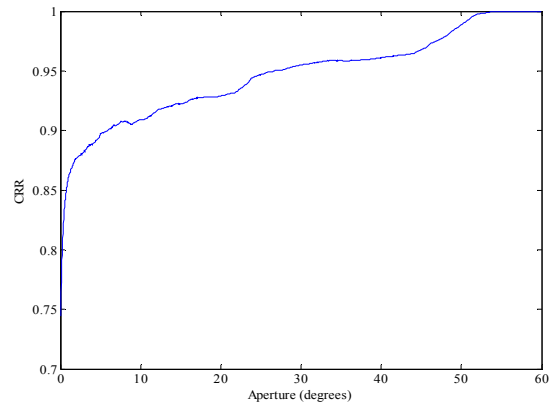


Figure 4: Cumulative multi-perspective correct classification rates versus covered aperture

In Figure 4, the classification performance of the cumulative classifier is shown for an aperture  $\phi = 60^\circ$  (i.e. the radar is “on” for almost one minute). After the rapid augmentation of the CRR due to the progressive signatures decorrelation, the updated score increases linearly with the synthesised aperture ( $\sim 5\%$  every  $25^\circ$ - $30^\circ$ ). The interrupted geometry is depicted in Figure 5. The radar system is “on” for a limited amount of time so that  $N$  profiles are collected. Then the system is switched off until the next perspective is reached.

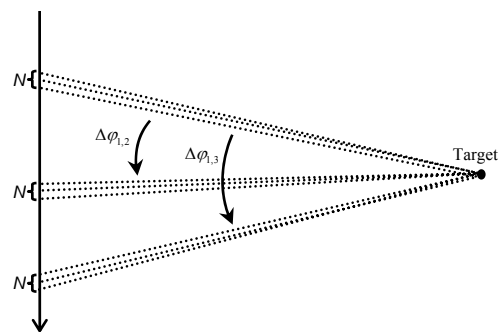
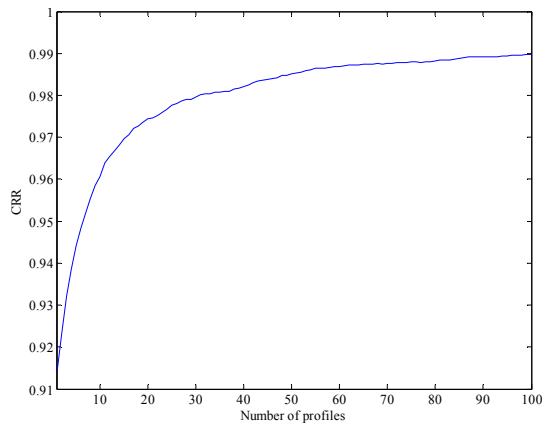


Figure 5: Interrupted acquisition for multi-perspective classification



**Figure 6:** *Interrupted multi-perspective CRR versus number of signatures per perspective*

The perspective displacements vector  $\Delta\varphi = \{\Delta\varphi_{1,2}; \Delta\varphi_{1,3}\}$  is chosen on the basis of the best *CRR* obtained for a three perspective classifier for a total aperture of  $60^\circ$ . This is verified when  $\Delta\varphi = \{28^\circ; 60^\circ\}$ , and *CRR* = 91.6%. As can be observed in Figure 6, where the three-perspective *CRR* is plotted versus  $N$ , the classification rate stabilises for  $N \geq 40$ . This is achieved when the radar is “on” for a time  $t \sim 1$  s for each perspective. In this case the classifier shows a probability of correct classification comparable to the cumulative classifier after 40 seconds of data acquisition. The rapid increase of *CRR* is due to the decorrelation of the consecutive signatures within each perspective.

### Conclusion

In this work, the effect of the perspective aperture between multiple looks of the target has been presented as well as a potential implementation of the multi-perspective classifier. In a two-perspective scenario, every small departure from the collocation of the sensors gives a very marked improvement in classification performance. A  $90^\circ$  separation has been found to be not quite optimum, because it could associate the end-on profile with the broadside profile, both likely to be swamped by specular reflections. Hence a separation of  $100^\circ$  to  $110^\circ$  is generally a good choice. Conversely, considering three nodes, the

best correct classification rates are achieved when the perspectives are evenly spaced around the target. Nevertheless, the probability of correct classification averaged over any possible network topology is well above the mono-perspective case (+11.3% and 15.5% using two and three perspectives respectively).

### References

- 1 Rong Hu, Zhaoda Zhu, 1997, IEEE Aerospace and Electronics Conference, **2**, 951-955.
- 2 Novak, L. M., Halversen, S. D., Owirka, G., Hiett, M., 1997, IEEE Transactions on Aerospace and Electronic Systems, **33**, Issue 1, 102-116.
- 3 Sadjadi, F., 2002, IEEE Transactions on Aerospace and Electronic Systems, **38**, Issue 1, 38-49.
- 4 Shihao Ji, Xuejun Liao, Carin, L., 2005, IEEE Sensors Journal, **5**, Issue 5, 1035-1042.
- 5 Xuejun Liao, Runkle, P., Carin, L., 2002, IEEE Transactions on Aerospace and Electronic Systems, **38**, Issue 4, 1230-1242.
- 6 Runkle, P. R., Bharadwaj, P. K., Couchman, L.; Carin, 1999, IEEE Transactions on Signal Processing, **47**, Issue 7, 2035-2040.
- 7 Vespe, M., Baker, C. J. Griffiths H. D., 2005, EMRS-DTC 2<sup>nd</sup> Technical Conference.
- 8 Xiao Huaitie et al., 1997, Aerospace and Electronics Conference, **2**, 764-768.
- 9 Theodoridis, S., Outroumbas, 1999, Pattern Recognition, Academic Press.

### Acknowledgements

The work reported in this paper was funded by the Electro-Magnetic Remote Sensing (EMRS) Defence Technology Centre, established by the UK Ministry of Defence and run by a consortium of SELEX Sensors and Airborne Systems, Thales Defence, Roke Manor Research and Filtronic.